Soft Matter

RSC Publishing

PAPER

View Article Online
View Journal | View Issue

Cite this: *Soft Matter*, 2013, **9**, 7086

Monte Carlo simulation of thermo-responsive charged nanogels in salt-free solutions

Manuel Quesada-Pérez*[a] and Alberto Martín-Molina[b]

In this work, we have performed explicit coarse-grained Monte Carlo simulations of thermo-responsive nanogels in salt-free solutions with the help of the bead-spring model of polyelectrolytes and a solvent-mediated hydrophobic interaction potential that captures the swelling behavior of real microgels. As far as we know, such simulations have not been applied to temperature-sensitive charged nanogels yet. Monovalent and divalent counterions have been considered. Charge profiles inside and outside the nanogel have been computed from simulations, revealing an attractive finding for the use of these nanoparticles as potential drug carriers: when charged nanogels collapse, they can sometimes form a hollow sphere, with the charged beads concentrated on the inner and outer surfaces, and some counterions enclosed in the inner space. Simulations also show that the surface electrostatic potential increases when nanogels shrink upon heating. However, the fraction of counterions inside these soft nanoparticles slightly varies with temperature. Charge profiles were also calculated using a Poisson–Boltzmann cell model. Its predictions about the charge profile outside the nanogel, the fraction of counterions inside and the surface electrostatic potential are in fair agreement with simulation data. This suggests that this model provides valuable information about the electric double layer of thermo-responsive nanogels.

Received 10th January 2013
Accepted 17th April 2013

DOI: 10.1039/c3sm00093a

www.rsc.org/softmatter

Introduction

Since 1986, there have been many publications describing the preparation, characterization and application of temperature-sensitive microgels. These smart materials have been the subject of many investigations due to their potential biotechnological applications (for instance, in drug delivery).[1,2] The small size of nano- and microgels enables them to develop a rapid kinetic response to temperature changes as well as other stimuli (such as pH).

From a theoretical viewpoint, thermo-responsive microgels have been generally studied through the classical formalism of macroscopic gel swelling (see ref. 3 and references quoted there for further information). Very recently, the real behavior of poly(*N*-isopropylacrylamide) [poly(NIPAM)] based microgels containing different quantities of acrylic acid has also been analyzed with the help of computer simulations and a bead-spring model of polyelectrolytes, which has been widely applied to gels and other polyelectrolyte assemblies in the last decade.[4–21]

But the reader should keep in mind that the models used in the classical formalism and simulations assume that the polymer/polyelectrolyte network is infinite. This assumption could be reasonable for macroscopic gels and even for microgels if they are large enough, but it seems questionable for networks of a few nanometers (nanogels). In any case, it involves two additional important limitations for nanogels: (i) the counterions that neutralize the gel charge must reside inside the network and (ii) it is not possible to consider the ionic atmosphere (the electric double layer) around the nanogel. Thus the classical formalism of gel swelling is not useful from a colloidal perspective because it cannot provide information about important particle properties such as size, effective charge or surface electrostatic potential. For similar reasons, the classical formalism of swelling cannot be applied to study the colloidal interactions between two nanogels either.

In spite of these limitations, nanogels have been very scarcely simulated. Claudio *et al.* have shown that nanogels do not confine their counterions completely.[22] They also compare the predictions of a Poisson–Boltzmann (PB) cell model with molecular dynamics data, concluding that the ion distributions predicted by this model and those obtained from simulations agree quite well. But their survey is restricted to good solvent conditions and monovalent ions. On the other hand, Jha *et al.* have used the theoretically informed coarse-grained simulation approach, which has been developed in the context of block copolymer melts.[18] This novel approach also describes the polymer chains in a coarse-grained fashion together with a particle-formalism for the treatment of bonded interactions and

[a]*Departamento de Física, Escuela Politécnica Superior de Linares, Universidad de Jaén, 23700, Linares, Jaén, Spain. E-mail: mquesada@ujaen.es*

[b]*Grupo de Física de Fluidos y Biocoloides, Departamento de Física Aplicada, Facultad de Ciencias, Universidad de Granada, 18071 Granada, Spain*

a field-formalism for the treatment of non-bonded interactions. In any case, the explicit thermal response of temperature-sensitive nanogels was not studied in these two references and, as far as we know, it has not been simulated yet.

In view of that, our main goal is to look into the swelling of temperature-sensitive nanogels. The thermo-responsive behavior is simulated with the help of a solvent-mediated hydrophobic interaction potential that reproduces experimental swelling data of microgels.[20] We will also pay special attention to the distribution of counterions inside and outside these soft nanoparticles, extending the work of Claudio *et al.* to collapsed nanogels and the case of divalent counterions. The motivation for this extension is twofold. On the one hand, it is widely known that the PB approach can fail in the description of the electric double layer of hard colloidal particles if multivalent counterions are present.[23] Hence it would be desirable to analyze this possibility in the case of soft nanoparticles. On the other hand, as potential therapeutic carriers, nanogels could absorb biocompatible divalent ions such as Ca^{2+} and Mg^{2+}. For instance, the self-assembly behavior of nanogels formed with polymers of poly-*block*-poly(methacrylic acid) involves Ca^{2+} ions.[24] Thus it would be interesting to explore how such ionic species can modify the thermal response.

The rest of the paper is organized as follows. First, the bead-spring model of nanogels used here and the PB cell model are described. Some technical details on simulations are briefly discussed. Then, some results on the thermal response, the charge profiles, the fraction of counterions inside the network, and the electrostatic potential are given. Finally, some conclusions are highlighted.

Model and simulations

Bead-spring model of nanogels

The nanogel is described within a bead-spring model, which is quite similar to that employed by Claudio *et al.*, together with the primitive model.[22] Consequently, the solvent is taken into account only through its dielectric permittivity. The assumption of the primitive model has been extensively used in simulations of gels and nanogels (even when these polyelectrolyte networks are highly shrunken) because simulating the solvent explicitly is prohibitively expensive for the length scales and time scales of interest. However, there are some signs supporting the primitive model for certain purposes. For instance, in a previous work we found that the swelling behavior of microgels with 8 monomers per chain can be acceptably captured with a constant dielectric permittivity.[20] For free polymers, some authors have compared explicit solvent simulations and certain promising implicit solvent models.[25,26]

Each chain is modeled as a sequence of n_{bead} spherical monomer units (beads) connected by tetrafunctional cross-linkers (also modeled by identical beads). This survey is restricted to $n_{bead} = 4$. Our nanogel has 133 cross-linkers, 70 of them (the inner ones) are actually connected to four polyelectrolyte chains. But the rest can be connected only to three, two and even one chain (especially those more external). The total number of chains is 206. One bead of each chain is charged with the negative elementary charge ($-e$). This charged bead is located in the position 2 (or 3) of the chain trying to separate the charged monomers as much as possible and generate a roughly uniform distribution. Fig. 1a shows the nanogel in the initial configuration, whose internal structure exhibits the diamond-like topology used in the simulations of macroscopic gels. However, Fig. 1a also shows some dangling outer chains. Once the particles are allowed to move, the shape becomes more spherical (Fig. 1b). The simulation cell must also include the number of counterions required to neutralize the nanogel charge. The presence of additional counterions and co-ions is not considered here. As mentioned before, monomer units of polymer chains, cross-linker molecules and counterions are explicitly modeled as spheres, whose diameters are σ_M, σ_{CL} and σ_{CI}, respectively. The same value was assumed for the diameters of monomer units and cross-linker molecules ($\sigma_M = \sigma_{CL} = 0.65$ nm).[20] For ions, the size includes the corresponding hydration shell. In the case of monovalent counterions, we have

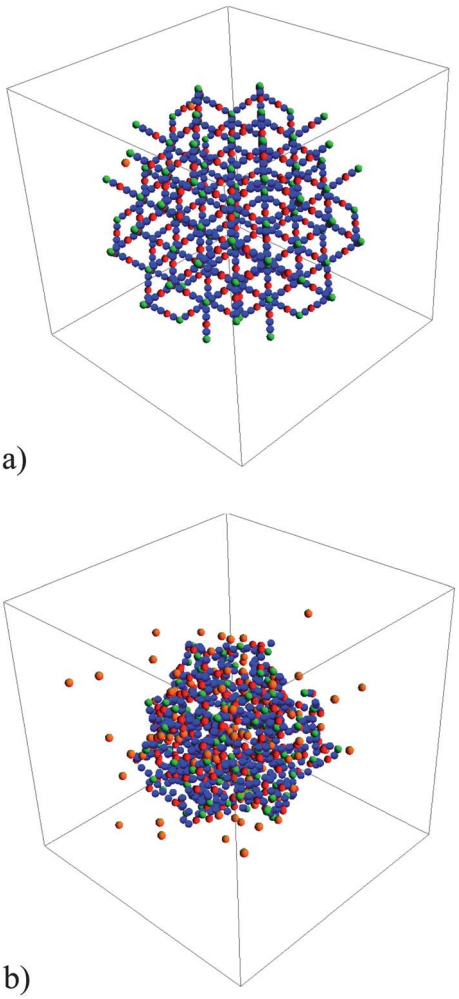

Fig. 1 Snapshots of the nanogel in the presence of monovalent counterions: (a) initial configuration; (b) at 288 K after thermalization. Blue, red, green and orange spheres symbolize uncharged beads, charged beads, cross-linkers and counterions, respectively. The box (with sides of 25 nm) represents only the central part of the simulation cell.

adopted $\sigma_{CI} = 0.7$ nm, a value obtained by averaging different estimations from experimental techniques.[27] For divalent ions we have performed simulations with two different ionic diameters. As a first option, we have also used 0.7 nm. The estimated values for divalent cations are slightly greater,[27] but the effect of the ionic valence can be more easily analyzed if the ionic size remains fixed. In addition, we would like to explore the effect of ionic size for divalent cations, since their hydration shell might reduce when they are bound to charged monomeric units. For that reason, we have also carried out simulations with $\sigma_{CI} = 0.4$ nm.

Interactions

The short-range repulsion between any pair of these particles due to excluded volume effects can be modeled by means of a truncated Lennard-Jones potential:[9–11,28]

$$u_{LJ}(r) = \begin{cases} 4\varepsilon_{LJ}\left(\frac{\sigma^{12}}{r^{12}} - \frac{\sigma^{6}}{r^{6}} - c\right) & r \le r_c \\ 0 & r > r_c \end{cases} \quad (1)$$

where r is the center-to-center distance between a given pair of particles (i and j), $\varepsilon_{LJ} = 4.11 \times 10^{-21}$ J, $\sigma = (\sigma_i + \sigma_j)/2$, r_c is the cut-off distance and c is a constant chosen so that $u_{LJ}(r_c) = 0$. If $r_c = 2^{1/6}\sigma$ the interaction potential is purely repulsive. Monomer units and cross-linkers are connected with their neighbors by harmonic bonds:[4,7,12,13]

$$u_{bond}(r) = \frac{k_{bond}}{2}(r - r_0)^2 \quad (2)$$

where k_{bond} is the elastic constant ($k_{bond} = 0.4$ N m^{-1}) and r_0 ($= 0.65$ nm) is the equilibrium bond length.

All the charged species (monomers and ions) interact electrostatically through the Coulomb potential:

$$u(r) = \frac{Z_i Z_j e^2}{4\pi\varepsilon_0\varepsilon_r r} \quad (3)$$

where Z_i is the valence of species i, ε_0 and ε_r are the vacuum permittivity and relative permittivity of the solvent, respectively. Given that we are interested in the thermo-responsive nanogels, the temperature dependence of the dielectric permittivity is also considered:[29]

$$\varepsilon_r = \frac{5321}{T} + 233.76 - 0.9297T + 0.1417 \times 10^{-2}T^2 - 0.8292 \times 10^{-6}T^3 \quad (4)$$

The hydrophobic interaction

The interaction energy between nonbonded monomeric units is also considered in our model to capture the thermo-shrinking behavior, which is widely reported for gels and microgels. This potential would model attractive solvent-mediated hydrophobic forces, $u_{hyd}(r)$. The existence of these hydrophobic forces can be explained on molecular grounds as follows. When non-polar macromolecules are introduced into an aqueous medium, the water molecules form a structure (known as clathrate) around them, generating a lot of ordering.[3,19,30,31] The best way to avoid this loss of entropy is to keep all the non-polar molecules together in one globule, maximizing the volume-to-surface area ratio. It should be stressed, however, that the hydrophobic character of a substance is intrinsically temperature-sensitive. In other words, a nonpolar solute will aggregate only if the temperature exceeds a critical value. Below this value, the formation of clathrates is thermodynamically favored and the nonpolar solute is stably dispersed in water.

Admitting that the precise knowledge of such forces and their functional forms is far from complete, other authors have employed phenomenological potentials with different functional forms (square well, Lennard-Jones, and others) in previous simulations of flexible polymers.[32–38] For free polymers in poor solvents, Yethiraj and Reddy have recently tested the solvent-accessible surface area implicit solvent model by comparing with explicit solvent simulations and reporting hopeful results.[25,26] However, we must bear in mind that our survey is devoted to thermo-shrinking nanogels. Thus the model employed should consider a temperature-dependence that accounts for such thermal response. In a previous work,[19] we examined the pair potential proposed by Kolomeisky and Widom,[39] which encompasses the essential features of the hydrophobic mechanism (restricted orientations, ordering and energy release for solvent molecules near non-polar solutes). This potential predicts that hydrophobic forces must increase with the temperature. Unfortunately, our simulations revealed that the Kolomeisky–Widom (KW) potential overestimates the value of this interaction at high temperatures, yielding volume fractions larger than 1.[19] Accordingly, we propose here an empirical potential, which is a sigmoid approximation of the square-well potential used by other authors,[7,34,36] whose depth increases with temperature (the main feature of the KW potential) but reaches a maximum after a given temperature. This potential and its depth (ε_h) are described by the following functional forms:

$$u_{hyd}(r) = -\frac{\varepsilon_h}{2}(1 - \tanh(k_h(r - r_h))) \quad (5)$$

$$\varepsilon_h(T) = \frac{\varepsilon_{max}}{2}\left(1 + \tanh\left(k_{\varepsilon/2}(T - T_{\varepsilon/2})\right)\right) \quad (6)$$

where r_h is the range of the potential, k_h is related to the slope of the sigmoid, ε_{max} is the maximum depth of the hydrophobic potential (reached at high temperatures), $T_{\varepsilon/2}$ is the temperature for which $\varepsilon_h = \varepsilon_{max}/2$ and $k_{\varepsilon/2}$ is proportional to the slope of the function at that point. In this survey, the following values have been adopted for the potential parameters: $r_h = 0.9$ nm, $k_h = 12.2$ nm^{-1}, $T_{\varepsilon/2} = 307.5$ K, $k_{\varepsilon/2} = 0.0667$ K^{-1} and $\varepsilon_{max} = 7.5 \times 10^{-21}$ J. The values of r_h, k_h, $T_{\varepsilon/2}$ and $k_{\varepsilon/2}$ are identical to those used in a previous work to reproduce swelling data of poly-(NIPAM)-based microgels.[20] The value of ε_{max} is of the same order but intentionally larger to induce the formation of more collapsed charged nanogels. In addition, it should be mentioned that charged chemical groups are usually hydrophilic rather than hydrophobic. Thus the hydrophobic forces between beads with charged groups are likely to be considerably weakened. For that reason we have assumed, as a limiting case, that such hydrophobic interaction is not operative if any of the

interacting beads is charged. In any case, it should be mentioned that the model used here (inspired by thermo-shrinking microgels) is quite simple and quantitative comparisons with experiments (not considered in this paper) could require improvements.

Simulations

The simulations were performed using the canonical ensemble, in which volume and temperature are kept constant. All the simulations were carried out in a cubic box with a length $L =$ 100 nm and under periodic boundary conditions. The box size is fixed in this study. In practice, however, the value of L would be determined by the number concentration of nanogels (as usual in cell models).

Although there are efficient simulation packages, this work was carried out using our own computer code (in C). The Monte Carlo (MC) simulations were implemented by means of the Metropolis algorithm. Typically the maximum displacement is adjusted so that the average acceptance ratio is roughly 30–70%. In this case, however, the maximum displacements employed for counterions and network beads must be quite different. Only in this way, their respective acceptance ratios satisfy this criterion. It should also be mentioned that scaling moves were also attempted to accelerate the process of thermalization. In these moves, the positions of all the particles are scaled by multiplying by a factor α. After each one of these scaling moves, counterions tend to occupy the whole simulation cell again but the volume of the network would preferentially decrease. The acceptance probability for such scaling changes was therefore applied:[40]

$$P_{\alpha}^{\mathrm{acc}} = \min[1,\ \alpha^{3N}\exp(-\Delta U/k_{\mathrm{B}}T)] \tag{7}$$

where $P_{\alpha}^{\mathrm{acc}}$ is the probability that the coordinates of all particles are multiplied by α, N is the number of particles in the simulation cell and ΔU is the change in the potential energy. This quantity must be carefully calculated if long-range Coulomb forces are involved. In this work, Ewald sums were implemented with the recommendations suggested by Linse.[41] The calculation of the reciprocal contribution to energy requires the computation of the following sums

$$S(n_x, n_y, n_z) = \sum_{j=1}^{N} Z_j \exp\left[-i\left(\frac{2\pi n_x}{L}x_j + \frac{2\pi n_y}{L}y_j + \frac{2\pi n_z}{L}z_j\right)\right] \tag{8}$$

for a set of integers (n_x, n_y, n_z) that grows with accuracy. This task can become extremely time-consuming. Fortunately, only one summand is involved in one-particle MC displacements. Thus $S(n_x, n_y, n_z)$ can be more rapidly computed if it is initially calculated and stored for the whole set of integers and then easily recalculated for every single-particle move. For that reason, this kind of moves is exclusively attempted after thermalization.

1×10^8 and 2×10^8 configurations were used for thermalization and averaging, respectively. The evolution of the radius of gyration of the nanogel, R_{g}, was monitored by averaging this quantity in subbatches of 5×10^5 configurations to check that an equilibrium value was reached. The set of partially averaged R_{g}-values obtained after thermalization was also used to estimate the uncertainty of this quantity (as the standard deviation). Simulations also provide the concentration of charged particles at a distance r from the center of mass (CM), $n_{\mathrm{i}}(r)$, where i stands for counterions (CI) and charged beads.

PB cell model

The counterion profile was also computed from a PB approach applied to a spherical cell model of radius R_{cell}, whose volume is identical to that of the simulation box ($R_{\mathrm{cell}} = 62$ nm). Here the nanogel is modeled as a spherical object with the same radius obtained in the corresponding MC simulation (R_{NG}) and concentric with the spherical cell. We have assumed that the nanogel charge (Q_{NG}) is uniformly distributed. Counterions are allowed to move anywhere in the cell, even into the charged nanogel. In other words, this nanoparticle is assumed to be completely permeable to counterions. The concentration of counterions in the cell at a distance r from the center, $n_{\mathrm{CI}}(r)$, is calculated by solving the Poisson equation:

$$\nabla^2\psi(r) = -\frac{\rho(r)}{\varepsilon_0\varepsilon_{\mathrm{r}}} \tag{9}$$

where ψ is the electrostatic potential and ρ is the charge density, which is given by:

$$\rho(r) = \begin{cases} \dfrac{Q_{\mathrm{NG}}}{4\pi R_{\mathrm{NG}}^3/3} + Z_{\mathrm{CI}}e n_{\mathrm{CI}}(r) & r \le R_{\mathrm{NG}} \\ Z_{\mathrm{CI}}e n_{\mathrm{CI}}(r) & r > R_{\mathrm{NG}} \end{cases} \tag{10}$$

here Z_{CI} is the counterion valence. If it is also assumed that $\psi(R_{\mathrm{cell}}) = 0$, the counterion concentration can be written as the following Boltzmann distribution (coupled to the Poisson equation):

$$n_{\mathrm{CI}}(r) = n_{\mathrm{CI}}(R_{\mathrm{cell}})\exp(-Z_{\mathrm{CI}}e\psi) \tag{11}$$

This set of coupled equations was solved following the same procedure used in the classical scheme for hard colloids.[42]

Results and discussion

Thermal response

First, we will present the results of the effective radius of the nanogel (R_{NG}) as a function of the temperature. R_{NG} was determined from the radius of gyration of the network and the equation relating both quantities for a rigid sphere:

$$R_{\mathrm{NG}} = \sqrt{5/3}R_{\mathrm{g}} \tag{12}$$

Inspired by experiments with thermo-shrinking microgels of biotechnological interest, whose volume abruptly changes at physiological temperatures, we have explored the thermal response from 288 to 333 K. For this range of temperatures the Bjerrum length (defined as $l_{\mathrm{B}} \equiv e^2/4\pi\varepsilon_0\varepsilon_{\mathrm{r}}k_{\mathrm{B}}T$) slightly varies from 0.705 to 0.751 nm. These values are similar to the sizes of the monomer beads and one of the ionic diameters studied

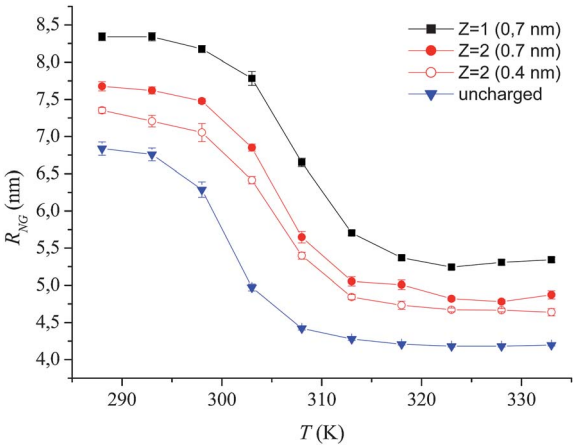

Fig. 2 Nanogel radius (at equilibrium) as a function of temperature in the presence of counterions with valence 1 (squares), valence 2 and a diameter of 0.7 nm (solid circles), valence 2 and a diameter of 0.4 nm (open circles). The results for the uncharged network are also shown for comparison (triangles).

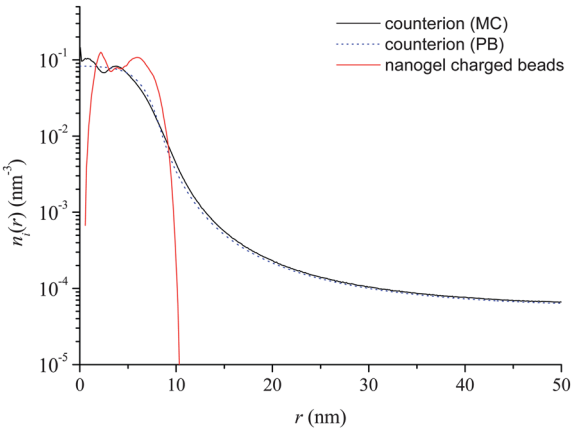

Fig. 3 Number concentration ($n_i(r)$) of charged beads and monovalent counterions as a function of the distance from the center of mass of the nanogel (r) at 288 K.

here (0.7 nm). Fig. 2 shows the nanogel radii obtained in the presence of monovalent and divalent counterions. In the case of divalent counterions, results for two ionic diameters are plotted. Data for an uncharged nanogel with identical numbers of chains, cross-linkers, beads per chain and topology are also included for comparison. In all the cases, the transition from the swollen to the collapsed state is described by a sigmoid curve, whose inflection point is interpreted by many experimentalists as a transition temperature. For instance, the transition temperature of the uncharged gel is about 303 K ($\approx$30 °C), which is close to that experimentally reported for poly(NIPAM) gels and microgels. As can be seen, the charged nanogel with Z_{CI} = +1 exhibits larger radii and a higher transition temperature. The larger swelling capacity of charged gels is usually attributed to the osmotic pressure exerted by the counterions (all of them reside inside the gel). This can also be valid for nanogels, although we should keep in mind that only a fraction of these counterions resides inside the nanogel. In spite of the reduction in the osmotic pressure, this feature would also explain the shift of the transition toward higher temperatures. What happens for divalent counterions? Our simulations reveal that the swelling of the nanogel is smaller and the transition temperature is less shifted than in the case of monovalent counterions. This is logical since the number of these ions required to neutralize gel charged groups is reduced to 50%. Fig. 2 also shows that the radii obtained for divalent counterions are a bit smaller when the ionic size is reduced from 0.7 to 0.4 nm. This minor ionic size effect could be related to the electrostatic bridging induced by multivalent ions, which could play the role of the cross-linking agents bringing charged chains together.[21,43,44] Such bridging would be enhanced when the size is reduced. In any case, the comparison of Fig. 2 with previously published results for infinite networks confirms that the effect of ionic valence is quite similar for gels and nanogels (at least, qualitatively speaking).[21]

Charge profiles

Fig. 3–6 show the concentration of charged beads and counterions as a function of the distance from the nanogel CM for four representative cases: 288 K and Z_{CI} = +1 (Fig. 3), 333 K and Z_{CI} = +1 (Fig. 4), 288 K and Z_{CI} = +2 (Fig. 5), 333 K and Z_{CI} = +2 (Fig. 6). For divalent counterions, only data for σ_{CI} = 0.7 nm were chosen. First, let us consider a moderately swollen nanogel in the presence of monovalent counterions (Fig. 3). As can be seen, the charge of this nanogel is not uniformly distributed and exhibits two maxima at 2.1 and 5.9 nm approximately. This suggests that the nanogel charge is structured in two concentric shells, whose origin could be related to the central (and nonrandom) positions of the charged beads in the chains. The figure also reveals that the CM of the nanogel is not occupied by charged beads but counterions. The profile of this species also exhibits peaks, which again suggests the existence of some ordering, but only in the inner region. In contrast, the counterion profile is monotonous out of the nanogel and decays

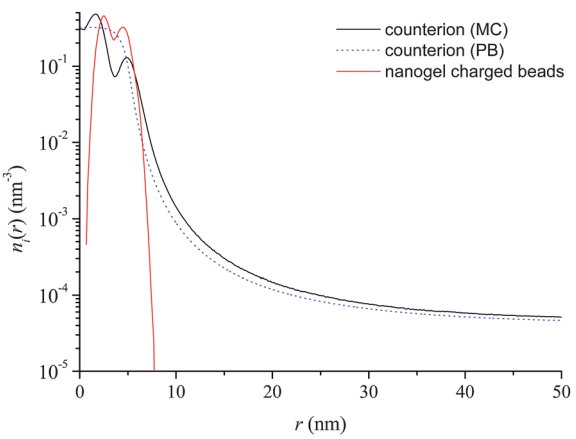

Fig. 4 Number concentration ($n_i(r)$) of charged beads and monovalent counterions as a function of the distance from the center of mass of the nanogel (r) at 333 K.

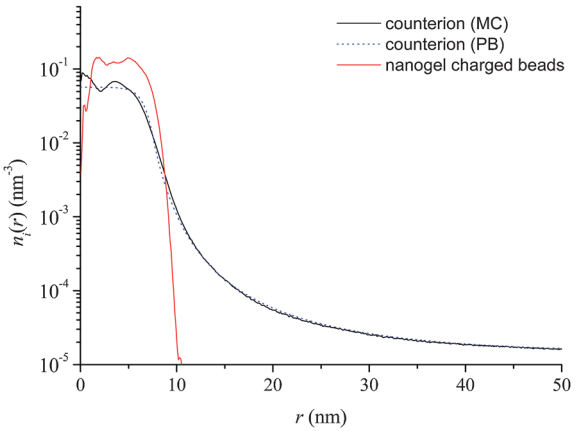

Fig. 5 Number concentration ($n_i(r)$) of charged beads and divalent counterions as a function of the distance from the center of mass of the nanogel (r) at 288 K.

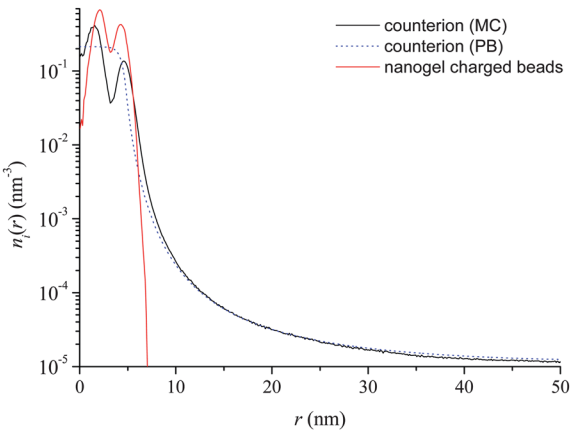

Fig. 6 Number concentration ($n_i(r)$) of charged beads and divalent counterions as a function of the distance from the center of mass of the nanogel (r) at 333 K.

rapidly with the distance. Fig. 3 also includes the prediction of the PB cell model, which was calculated using as nanogel radius the value obtained from simulation data. As can be seen, this model predicts a monotonous profile even inside the network, but this is not surprising since a uniform nanogel charge distribution was assumed. In the outer region, the qualitative and quantitative agreement between theory and simulation is excellent. From the counterion profile, we also calculated the fraction of this species inside the network (f_{CI}), assuming that the limit between the inner and the outer region is just the nanogel radius, obtaining 0.573 from MC simulations and 0.524 from the PB approach.

Fig. 4 shows the same functions for 333 K. When the temperature increases, the nanogel shrinks and the shells of charged beads come obviously closer. Regarding the PB cell model, the agreement between its prediction and simulation is not so good in this case, particularly in the inner region. Concerning the fraction of counterions inside the nanogel, we obtained $f_{CI} \approx 0.595$ for MC simulations and $f_{CI} \approx 0.630$ when the PB approach was applied. As can be seen, the PB predictions are again similar to simulation results, confirming that the assumptions of high counterion permeability and uniform nanogel charge distribution are reasonable for monovalent ions, even in the case of collapsed networks. In addition, the comparison between results for 288 and 333 K reveals that f_{CI} slightly varies with temperature.

Fig. 5 and 6 show the profiles corresponding to divalent counterions, for 288 and 333 K, respectively. Among their features, the excellent agreement between theory and simulation in the outer region of the nanogels, even for the collapsed network at 333 K, is noticeable. This contrasts with the results for monovalent counterions, whose agreement for the collapsed network was worse. In relation to this striking finding, we should take into account that the number of counterions is reduced to 50% when their valence is doubled. This reduction is expected to contribute to an ideal behavior.

We should also mention another interesting result concerning the charged bead distribution. First we will discuss the case of divalent counterions, since it can be more easily appreciated. Fig. 5 shows that the peaks in the charge bead profile are not clearly defined. In contrast, when the network shrinks, two well defined peaks appear (see Fig. 6), which are also observed for monovalent counterions. This means that the nanogel charge is clearly structured in two shells for shrunken networks. This difference can also be illustrated with

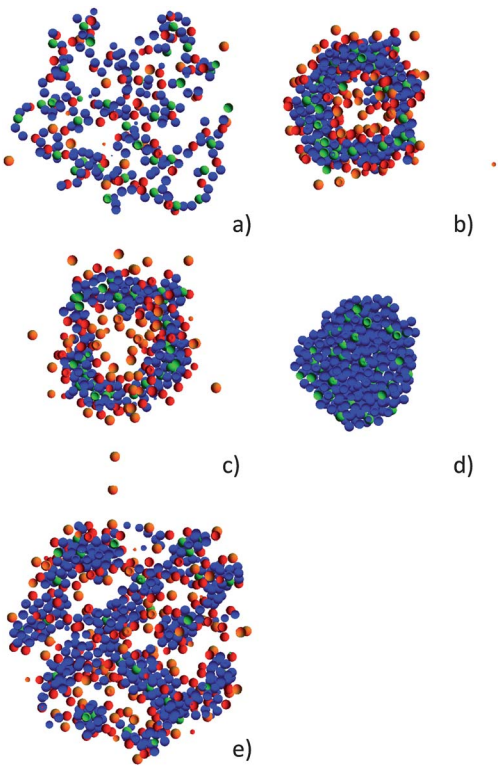

Fig. 7 Snapshots of slices of the central part of the simulation box with dimensions 2 nm × 20 nm × 20 nm to visualize cross-sections of the nanogels. (a) At 288 K with divalent counterions; (b) at 333 K with divalent counterions; (c) at 333 K with monovalent counterions; (d) at 333 K, for the uncharged nanogel. (e) Nanogel with $n_{bead} = 12$ and 3 charged beads per chain in the presence of divalent counterions at 333 K. Blue, red, green and orange spheres symbolize uncharged beads, charged beads, cross-linkers and counterions, respectively.

snapshots. Fig. 7 shows four *slices* of the central part of the simulation box with dimensions 2 nm × 20 nm × 20 nm, which permit us to visualize cross-sections of these soft nanoparticles at 288 and 333 K. In the case of the swollen network (288 K), neither charged beads nor counterions display an apparent spatial ordering (Fig. 7a). But the situation radically changes when the network collapses upon heating (Fig. 7b). As can be clearly seen, the nanogel forms a hollow sphere, with the charged beads concentrated on the inner and outer surfaces. In addition, counterions tend to be accumulated in the vicinity of these two surfaces. This result can be particularly appealing for the use of these nanoparticles as potential drug carriers, since collapsed nanogels could function as closed containers. For monovalent counterions we also found a similar behavior, but the structure is a bit less defined (see Fig. 7c). In any case, it should be stressed that charge plays a fundamental role in the formation of such hollow spheres. Fig. 7d shows the cross-section of an uncharged polymer network at 333 K. As can be easily concluded, the polymer beads are evenly distributed and do not form any hollow spheres. As mentioned previously, charged monomers are considered to be hydrophilic groups (rather than hydrophobic). Consequently, they are not attracted by the hydrophobic beads. In fact, when uncharged monomers collapse due to attractive hydrophobic forces, they would tend to segregate the hydrophilic groups as much as possible to minimize the free energy. The formation of an inner surface would contribute to an increase in the number of charged beads segregated. In other words, many of the hydrophilic beads would be displaced towards the outer and inner surfaces of the monomer clusters. This separation of hydrophilic and hydrophobic groups is to some extent similar to the widely known mechanism in the formation of some polyelectrolyte assemblies (such as micelles or liposomes).

The fraction of divalent counterions inside the nanogel was also calculated, obtaining 0.777 from MC simulations and 0.696 from the PB approach at 288 K. As in previous cases, both values reasonably agree. When the temperature increases to 333 K, the fraction of divalent counterions inside the nanogel was $f_{CI} \approx 0.730$ according to the MC profile and $f_{CI} \approx 0.764$ when the PB cell model was applied. These results support the acceptable agreement between theory and simulations once more. In addition, they confirm that: (i) the temperature dependence of this quantity is not significant and (ii) f_{CI} is larger for divalent counterions.

To end this subsection, it should be mentioned that gels can adopt very different conformations when they collapse,[17] and the hollow sphere reported here for nanogels is only one of those conformations. For instance, Fig. 7e shows the slice obtained if the number of beads per chain increases to 12 but the proportion of charged beads remains fixed. The topology of the conformation observed now is more complex. At first sight, it seems that there are several interconnected voids. This figure also reveals certain segregation of the charged beads, which are preferably exposed to the solvent. Apart from that, comparisons between explicit and implicit solvent simulations for free polyelectrolytes suggest that the clusters would be more loosely held in the presence of an explicit solvent.[45] In other words, these structures would not be so stable as inferred from simulations with implicit solvents. In any case, the study of such conformations goes beyond the scope of this survey.

Surface electrostatic potential

For soft nanoparticles, the slipping plane is not well defined and electrokinetic concepts such as the ζ-potential would not be easily related to electrokinetic measurable properties. However, the electrostatic potential in the nanogel surface can provide an approximate idea of the electrokinetic behavior. For that reason, we have computed $\psi(R_{NG})$, assuming again that the surface of these soft nanoparticles would be located at a distance R_{NG} from the CM. The electrostatic potential was computed by integration of the electric field, which in turn was obtained from Gauss' law and the charge profile. The MC results for monovalent and divalent counterions are plotted as a function of temperature in Fig. 8, together with the values predicted by the PB cell model. The surface electrostatic potentials obtained for divalent counterions are smaller (in magnitude) than those estimated for the monovalent ones. In any case, it should be stressed that the absolute value of the surface electrostatic potential increases with temperature following a sigmoid function, with the same region of rapid growth as the nanogel radius. This finding can be helpful to understand the electrostatic behavior of nano- and microgels. For instance, some authors have reported that the electrophoretic mobility of thermo-responsive microgels increases (in magnitude) with temperature according to a similar sigmoid function.[46] It should be mentioned, however, that the increase of the magnitude of the surface electrostatic potential is not straightforwardly related to an increase of the total charge. This can be easily elucidated as follows. If the fraction of counterions inside the nanogel slightly varies, the total charge enclosed by the nanoparticle surface should not significantly change. The PB predictions are qualitatively similar. Quantitatively speaking, the agreement between theory and simulations

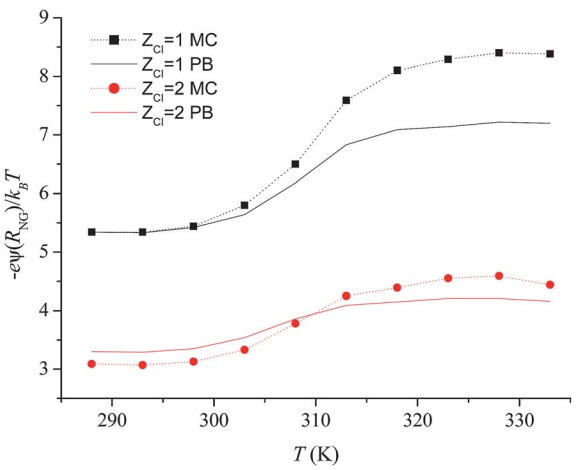

Fig. 8 Reduced surface electrostatic potential ($-e\psi(R_{NG})/k_BT$) as a function of temperature calculated from MC simulations for networks in the presence of monovalent and divalent counterions (squares and circles, respectively). The PB predictions are also shown (solid lines).

becomes worse for collapsed networks in the presence of monovalent counterions, just the case in which the greatest discrepancies in the counterion profiles were observed as well. In the explanation of these differences, the reader should also take into account that the electrostatic potential grows abruptly in approaching the surface. Thus larger numerical disagreements in $\psi(R_{NG})$ should be expected.

Finally, we should keep in mind that the distribution of charged beads employed here is roughly uniform. If charged beads were unevenly distributed, some quantitative and qualitative results could change. For instance, the agreement between the PB predictions and simulation results for counterion profiles could get worse. This is logical since the PB model assumes a uniform distribution of charged beads. In addition, the hollow sphere observed for some collapsed nanogels might become highly asymmetrical and even disappear.

Conclusions

Concerning the thermal response, our results qualitatively agree with those previously obtained for macroscopic gels. In particular, they confirm that the swelling decreases when monovalent counterions are replaced by divalent ones. In relation to the charge profiles, the simulations reveal that, in general, charged beads and counterions are not evenly distributed in the inner region of the nanogel. In particular, collapsed *charged* nanogels can sometimes form a hollow sphere, with the charged beads concentrated on the inner and outer surfaces, and some counterions enclosed in the inner space, corroborating that they could be used as closed drug containers. The partial segregation of uncharged beads (which tend to form clusters due to hydrophobic attractive forces) and charged beads (which are not attracted by the former) is probably the physical mechanism behind the formation of this hollow sphere and other more complex structures. We have also calculated the fraction of counterions inside the nanogel for swollen and collapsed networks, finding that this quantity slightly varies with temperature. Simulations also show that the surface electrostatic potential increases when thermo-responsive nanogels shrink upon heating.

In relation to the PB cell model, its predictions about the charge profile outside the nanogel, the fraction of counterions inside or the surface electrostatic potential are in reasonable agreement with simulations, even for collapsed nanogels and/or networks in the presence of divalent counterions. This suggests that the assumptions of high counterion permeability and uniform nanogel charge distribution are sound for the systems analyzed here. Thus, the PB cell model can provide reliable information about the electric double layer of thermo-responsive micro- and nanogels in salt-free solutions.

Acknowledgements

The authors are grateful for the financial support from the following institutions: (i) 'Ministerio de Ciencia e Innovación, Plan Nacional de Investigación, Desarrollo e Innovación Tecnológica (I+D+i)', Projects MAT2012-36270-C04-04 and -02 and (ii) 'Consejería de Innovación, Ciencia y Empresa de la Junta de Andalucía', Project P09-FQM-4698.

References

1 R. Pelton, *Adv. Colloid Interface Sci.*, 2000, **85**, 1–33.
2 J. Ramos, A. Imaz, J. Callejas-Fernandez, L. Barbosa-Barros, J. Estelrich, M. Quesada-Perez and J. Forcada, *Soft Matter*, 2011, **7**, 5067–5082.
3 M. Quesada-Perez, J. Alberto Maroto-Centeno, J. Forcada and R. Hidalgo-Alvarez, *Soft Matter*, 2011, **7**, 10536–10547.
4 S. Schneider and P. Linse, *J. Phys. Chem. B*, 2003, **107**, 8030–8040.
5 Q. L. Yan and J. J. de Pablo, *Phys. Rev. Lett.*, 2003, **91**, 018301.
6 Z. Y. Lu and R. Hentschke, *Phys. Rev. E: Stat., Nonlinear, Soft Matter Phys.*, 2003, **67**, 061807.
7 S. Schneider and P. Linse, *Macromolecules*, 2004, **37**, 3850–3856.
8 S. Edgecombe, S. Schneider and P. Linse, *Macromolecules*, 2004, **37**, 10089–10100.
9 B. A. Mann, R. Everaers, C. Holm and K. Kremer, *Europhys. Lett.*, 2004, **67**, 786–792.
10 B. A. Mann, C. Holm and K. Kremer, *J. Chem. Phys.*, 2005, **122**, 154903.
11 D. W. Yin, Q. L. Yan and J. J. de Pablo, *J. Chem. Phys.*, 2005, **123**, 174909.
12 S. Edgecombe and P. Linse, *Langmuir*, 2006, **22**, 3836–3843.
13 S. Edgecombe and P. Linse, *Macromolecules*, 2007, **40**, 3868–3875.
14 A. V. Dobrynin, *Curr. Opin. Colloid Interface Sci.*, 2008, **13**, 376–388.
15 D.-W. Yin, M. O. d. l. Cruz and J. J. d. Pablo, *J. Chem. Phys.*, 2009, **131**, 194907.
16 G. C. Claudio, K. Kremer and C. Holm, *J. Chem. Phys.*, 2009, **131**, 094903.
17 B. A. F. Mann, K. Kremer, O. Lenz and C. Holm, *Macromol. Theory Simul.*, 2011, **20**, 721–734.
18 P. K. Jha, J. W. Zwanikken, F. A. Detcheverry, J. J. de Pablo and M. O. de la Cruz, *Soft Matter*, 2011, **7**, 5965–5975.
19 M. Quesada-Pérez, J. G. Ibarra-Armenta and A. Martín-Molina, *J. Chem. Phys.*, 2011, **135**, 094109.
20 M. Quesada-Perez, J. Ramos, J. Forcada and A. Martin-Molina, *J. Chem. Phys.*, 2012, **136**, 244903–244909.
21 M. Quesada-Perez, J. A. Maroto-Centeno and A. Martin-Molina, *Macromolecules*, 2012, **45**, 8872–8879.
22 G. C. Claudio, K. Kremer and C. Holm, *J. Chem. Phys.*, 2009, **131**, 094903.
23 S. Madurga, A. Martín-Molina, E. Vilaseca, F. Mas and M. Quesada-Pérez, *J. Chem. Phys.*, 2007, **126**, 234703.
24 H. R. Sondjaja, T. A. Hatton and K. C. Tam, *Langmuir*, 2008, **24**, 8501–8506.
25 G. Reddy and A. Yethiraj, *Macromolecules*, 2006, **39**, 8536–8542.
26 G. Reddy and A. Yethiraj, *J. Chem. Phys.*, 2010, **132**, 074903.
27 J. N. Israelachvili, *Intermolecular and surface forces*, Academic Press, London; San Diego, 1991.

28 D.-W. Yin, F. Horkay, J. F. Douglas and J. J. de Pablo, *J. Chem. Phys.*, 2008, **129**, 154902.
29 *CRC handbook of chemistry and physics*, ed. D. R. Lide, CRC Press, 1988.
30 H. S. Frank and M. W. Evans, *J. Chem. Phys.*, 1945, **13**, 507–532.
31 W. Kauzmann, *Adv. Protein Chem.*, 1959, **14**, 1–63.
32 J. A. Anderson and A. Travesset, *Macromolecules*, 2006, **39**, 5143–5151.
33 P. Chodanowski and S. Stoll, *J. Chem. Phys.*, 1999, **111**, 6069–6081.
34 F. A. Escobedo and J. J. d. Pablo, *J. Chem. Phys.*, 1996, **104**, 4788–4801.
35 P. G. Khalatur, A. R. Khokhlov, D. A. Mologin and P. Reineker, *J. Chem. Phys.*, 2003, **119**, 1232–1247.
36 M. O. Khan, S. M. Mel'nikov and B. Jonsson, *Macromolecules*, 1999, **32**, 8836–8840.
37 N. Lee and D. Thirumalai, *Macromolecules*, 2001, **34**, 3446–3457.
38 U. Micka, C. Holm and K. Kremer, *Langmuir*, 1999, **15**, 4033–4044.
39 A. B. Kolomeisky and B. Widom, *Faraday Discuss.*, 1999, **112**, 81–89.
40 D. Frenkel and B. Smit, *Understanding Molecular Simulation: From Algorithms to Applications*, Academic Press, Inc., 1996.
41 P. Linse, in *Advanced Computer Simulation Approaches for Soft Matter Sciences II*, ed. C. Holm and K. Kremer, Springer-Verlag Berlin, Berlin, 2005, vol. 185, pp. 111–162.
42 S. Alexander, P. M. Chaikin, P. Grant, G. J. Morales, P. Pincus and D. Hone, *J. Chem. Phys.*, 1984, **80**, 5776–5781.
43 A. V. Ermoshkin and M. O. de la Cruz, *Phys. Rev. Lett.*, 2003, **90**, 125504.
44 A. V. Ermoshkin and M. O. De la Cruz, *J. Polym. Sci., Part B: Polym. Phys.*, 2004, **42**, 766–776.
45 R. W. Chang and A. Yethiraj, *Macromolecules*, 2006, **39**, 821–828.
46 T. Lopez-Leon, J. L. Ortega-Vinuesa, D. Bastos-Gonzalez and A. Elaissari, *J. Phys. Chem. B*, 2006, **110**, 4629–4636.